
This is an electronic reprint of the original article.
This reprint may differ from the original in pagination and typographic detail.

Chen, Min; Wan, Xingbang; Taskinen, Pekka; Sukhomlinov, Dmitry; Shi, Junjie; Michallik, Radoslaw; Jokilaakso, Ari

Phase equilibria in TiO₂-rich part of the MgO–CaO–TiO₂ system at 1500–1600 °C

Published in:
Ceramics International

DOI:
[10.1016/j.ceramint.2022.03.290](https://doi.org/10.1016/j.ceramint.2022.03.290)

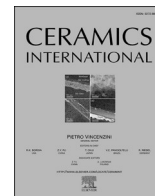
Published: 15/07/2022

Document Version
Publisher's PDF, also known as Version of record

Published under the following license:
CC BY

Please cite the original version:
Chen, M., Wan, X., Taskinen, P., Sukhomlinov, D., Shi, J., Michallik, R., & Jokilaakso, A. (2022). Phase equilibria in TiO₂-rich part of the MgO–CaO–TiO₂ system at 1500–1600 °C. *Ceramics International*, 48(14), 20116-20125. <https://doi.org/10.1016/j.ceramint.2022.03.290>

This material is protected by copyright and other intellectual property rights, and duplication or sale of all or part of any of the repository collections is not permitted, except that material may be duplicated by you for your research use or educational purposes in electronic or print form. You must obtain permission for any other use. Electronic or print copies may not be offered, whether for sale or otherwise to anyone who is not an authorised user.



Phase equilibria in TiO₂-rich part of the MgO–CaO–TiO₂ system at 1500–1600 °C

Min Chen^a, Xingbang Wan^{a,b,*}, Pekka Taskinen^a, Dmitry Sukhomlinov^a, Junjie Shi^{c,d}, Radoslaw Michallik^e, Ari Jokilaakso^a

^a Department of Chemical and Metallurgical Engineering, School of Chemical Engineering, Aalto University, Kemistintie 1F, P.O. Box 16100, FI-00076, Aalto, Finland

^b School of Energy Science and Engineering, Central South University, Changsha, 410083, China

^c School of Metallurgy, Northeastern University, Shenyang, 110819, China

^d Key Laboratory for Ecological Metallurgy of Multimetallic Mineral (Ministry of Education), Northeastern University, Shenyang, 110819, China

^e Geological Survey of Finland, Vuorimiehentie 2, 02150, Espoo, Finland

ARTICLE INFO

Keywords:

Titania-bearing slag
Phase equilibria
Resource efficiency
Thermodynamics
Phase diagram
TiO₂

ABSTRACT

The equilibrium phase relations of the MgO–CaO–TiO₂ system were investigated at 1500–1600 °C in air using the high-temperature isothermal equilibration of samples in platinum crucibles followed by the rapid quenching technique. The phase compositions were analyzed using an electron probe X-ray microanalyzer (EPMA). The isothermal sections at 1500 °C and 1600 °C were constructed based on the experimentally determined liquid phase compositions. The present results deviate significantly from previous observations as well as the predictions by MTDATA and FactSage using their oxide databases, in particular in the perovskite primary phase field.

1. Introduction

Titanium alloys are widely used in the fields of aviation, aerospace, medicine, and construction [1], for example, due to their properties of low density, high strength, good corrosion resistance, and non-toxicity [2]. The production of titanium from its mineral ores involves the carbochlorination of rutile and ilmenite to obtain TiCl₄, followed by metallothermic reduction with magnesium [3,4]. However, large amounts of energy consumption and greenhouse gas emissions are associated with this production process. Thus, a cleaner and more efficient way of titanium production is required.

With the increased awareness of environment protection and a growing demand for a circular economy, the utilization of secondary materials to recover valuable metals [5–9] has attracted more attention. Titania-bearing blast furnace slag, which is one of the largest metallurgical wastes containing 22–25 wt% TiO₂ [10–12], has become an important resource of titania [13]. The CaO–SiO₂–Al₂O₃–MgO–TiO₂ system can be used to describe the industrial titania-bearing blast furnace slags based on their chemical composition [14–28]. Investigation of the phase equilibria relations of the TiO₂-bearing sub-ternary

systems helps to deepen our understanding of the higher order systems, and subsequently promotes the utilization of blast furnace slags [29–32].

Abundant data are available for the phase relations of the sub-binary systems of CaO–MgO [33–41], CaO–TiO₂ [42,43], and MgO–TiO₂ [44–47]. However, it seems that there are limited fundamental data available on the CaO–MgO–TiO₂ system. Coughanour et al. [48] have determined the binary joints in the CaO–MgO–TiO₂ system at 1450–1750 °C using the quenching technique and phase characterization by X-ray and petrographic, although the liquid domain information was not reported in their study. Rouf et al. [49] have investigated the CaO–TiO₂–MgO–TiO₂–TiO₂ portion of the CaO–MgO–TiO₂ system using a hot-stage microscope, micro-differential thermal analysis, and X-ray diffraction techniques. The liquidus temperatures were determined using 5 wt% Rh–Pt/20 wt% Rh–Pt thermocouples. However, they reported that the hot-stage microscope method was not reliable for samples with a TiO₂ content of less than 70 wt%. Furthermore, the method of DTA and visual observations in a hot-stage microscope during cooling the sample with a high cooling rate (10–90 °C/min) brought the difficulties of reaching real equilibrium. They reported the

* Corresponding author. Kemistintie 1F, P.O. Box 16100, FI-00076, Aalto, Finland.

E-mail addresses: minchen0901@hotmail.com, min.chen@aalto.fi (M. Chen), xingbangwan@126.com (X. Wan), pekka.taskinen@aalto.fi (P. Taskinen), dmitry.sukhomlinov@aalto.fi (D. Sukhomlinov), junjieshi@126.com (J. Shi), radoslaw.michallik@gtk.fi (R. Michallik), ari.jokilaakso@aalto.fi (A. Jokilaakso).

<https://doi.org/10.1016/j.ceramint.2022.03.290>

Received 24 November 2021; Received in revised form 29 March 2022; Accepted 29 March 2022

Available online 2 April 2022

0272-8842/© 2022 The Authors. Published by Elsevier Ltd. This is an open access article under the CC BY license (<http://creativecommons.org/licenses/by/4.0/>).

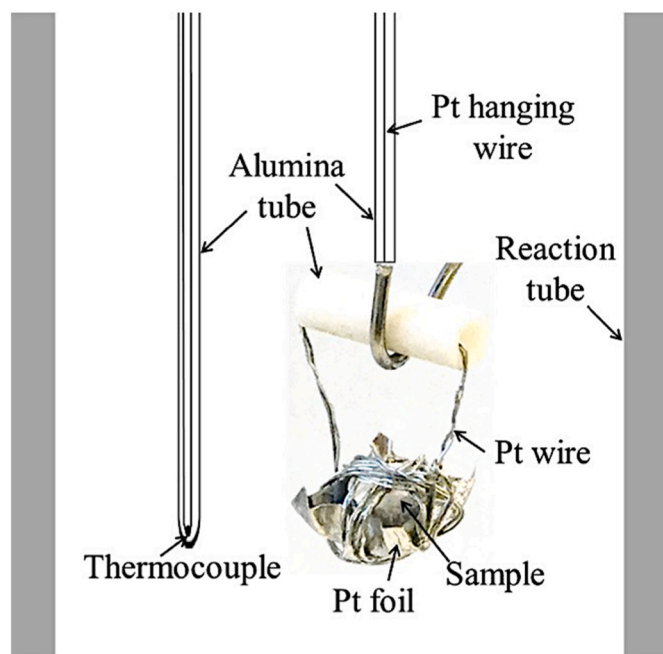


Fig. 1. A schematic diagram of the sample suspension technique.

repeatability/accuracy of their temperature data from ± 5 to ± 10 °C but without examining the effect of cooling rate. Typically, dynamic methods result in lower liquidus temperatures due to undercooling, but that effect was not studied. Shultz [50] have determined the solidus relations of the CaO–MgO–TiO₂ system over the temperature range 1407–1670 °C in air using the quenching method.

In summary, the phase relations of the MgO–CaO–TiO₂ system have not been investigated systematically. Therefore, this study aimed to investigate the phase equilibria of the MgO–CaO–TiO₂ system at 1500–1600 °C in air using the high-temperature equilibration/quenching/SEM-EDS/EPMA technique. The acquired experimental phase equilibrium data are useful for optimizing the thermodynamic properties in higher-order systems.

2. Experimental

The slag mixtures were prepared using high purity powders of CaO (99.9 wt%, Sigma-Aldrich), MgO (99.95 wt%, Alfa Aesar), and TiO₂ (99.8 wt%, Sigma-Aldrich). For each sample, the powders were weighed in an appropriate ratio, mixed in an agate mortar, and then pressed into a pellet using a hydraulic press. Approximately 0.2 g of molten sample was equilibrated at high temperature for each experiment.

The experiments involved high-temperature isothermal equilibration, quenching in an ice-water mixture, and phase characterization by SEM-EDS/EPMA on polished sections. The high-temperature equilibration of samples was conducted in a vertical tube furnace (Nabertherm, RHTV 40–250/18, Germany) equipped with silicon carbide heating elements. A calibrated S-type Pt/Pt-10% Rh thermocouple was placed next to the sample to measure the sample temperature, as shown in Fig. 1. The samples were pre-melted at a temperature 50 °C higher than the equilibration temperature for 30 min and then lowered to 1500 °C or 1600 °C for equilibration. It had already been proved in our previous studies that at experimental temperatures the system can reach equilibrium within 24 h [18,28,51]. Therefore, all samples were annealed at high temperature for at least 24 h. After equilibration, the sample was

quenched in an ice-water mixture, dried in air, mounted in epoxy, ground, and polished by wet metallographic methods, and carbon-coated using a carbon vacuum evaporator (LEICA EM SCD050, Austria). The experimental techniques have been described in detail in our previous papers [52–54].

The microstructures and phase compositions of samples were pre-examined using a scanning electron microscope (SEM, Tescan MIRA 3, Brno, Czech Republic) coupled with an UltraDry Silicon Drift Energy Dispersive X-ray Spectrometer (EDS, Thermo Fisher Scientific, Waltham, MA, USA). The elemental compositions of all phases were accurately determined using a Cameca SX100 Electron Microprobe (Cameca SAS, Genevilliers, France) using the Wavelength Dispersive Spectrometers (WDS). The operation parameters for EPMA analyses were accelerating voltage of 20 kV and beam current of 60 nA. A defocused beam diameter set to 50 μm for the liquid phase and 10–20 μm for the solid phase was used. The standards employed for EPMA were naturally occurring minerals rutile for O K α and Ti K α , diopside for Mg K α , and bustamite for Ca K α . The PAP-ZAF matrix correction procedure [55] was used for the raw data processing. At least 8 points were selected from the well quenched area of each phase in the EPMA and EDS analyses. The standard deviation ($\pm 1\sigma$) of the EPMA measurements is shown as uncertainty of each point.

3. Results

3.1. Equilibrium phase relations at 1500 °C

The microstructures and phase compositions of samples obtained at 1500 °C are shown in Fig. 2 and Table 1, respectively. The valence state of titanium in samples equilibrated in air has been investigated in our previous studies [51,53,54] by XPS, XRD, and the Ti–O stability phase diagram. The main titanium oxide species in the slags in air was found to be TiO₂. Therefore, the concentration of titanium oxide in the present study was calculated from the primary data as TiO₂. Several liquid-solid phase equilibria (*i.e.*, liquid-rutile, liquid-pseudobrookite, and liquid-perovskite) and three-phase equilibria, including liquid-rutile-pseudobrookite and liquid-ilmenite-perovskite, were observed at 1500 °C.

The relationship between the number of phases and the number of components of an equilibrium system can be obtained from the Gibbs phase rule [56]:

$$F = C - P + 2 \quad (1)$$

where F refers to the variance of freedom, C = the number of independent components, and P = the number of phases. The number 2 represents the temperature and total pressure of the investigated system. In the present study with fixed temperature and total pressure $P_{\text{total}} = 1$ atm, Eq. (1) can be simplified as Eq. (2):

$$F = C - P \quad (2)$$

The number of independent components C in the ternary system investigated in the present study is 3, including CaO, MgO, TiO₂. The number of coexisting phases P is 3 for the liquid-rutile-pseudobrookite three-phase equilibrium observed in the present study. Therefore, the degree of freedom F could be finally confirmed as $F = 3 - 3 = 0$ under the present experimental conditions. As the liquid-rutile-pseudobrookite coexisting equilibrium was observed in samples MCT-3, MCT-5, and MCT-31, the compositions of the liquid and solid phases for liquid-rutile-pseudobrookite were determined as the average of samples MCT-3, MCT-5, and MCT-31, which gave compositions of 6.26 wt% MgO–81.72 wt% TiO₂–12.02 wt% CaO, 0.05 wt% MgO–99.94 wt% TiO₂–0.02

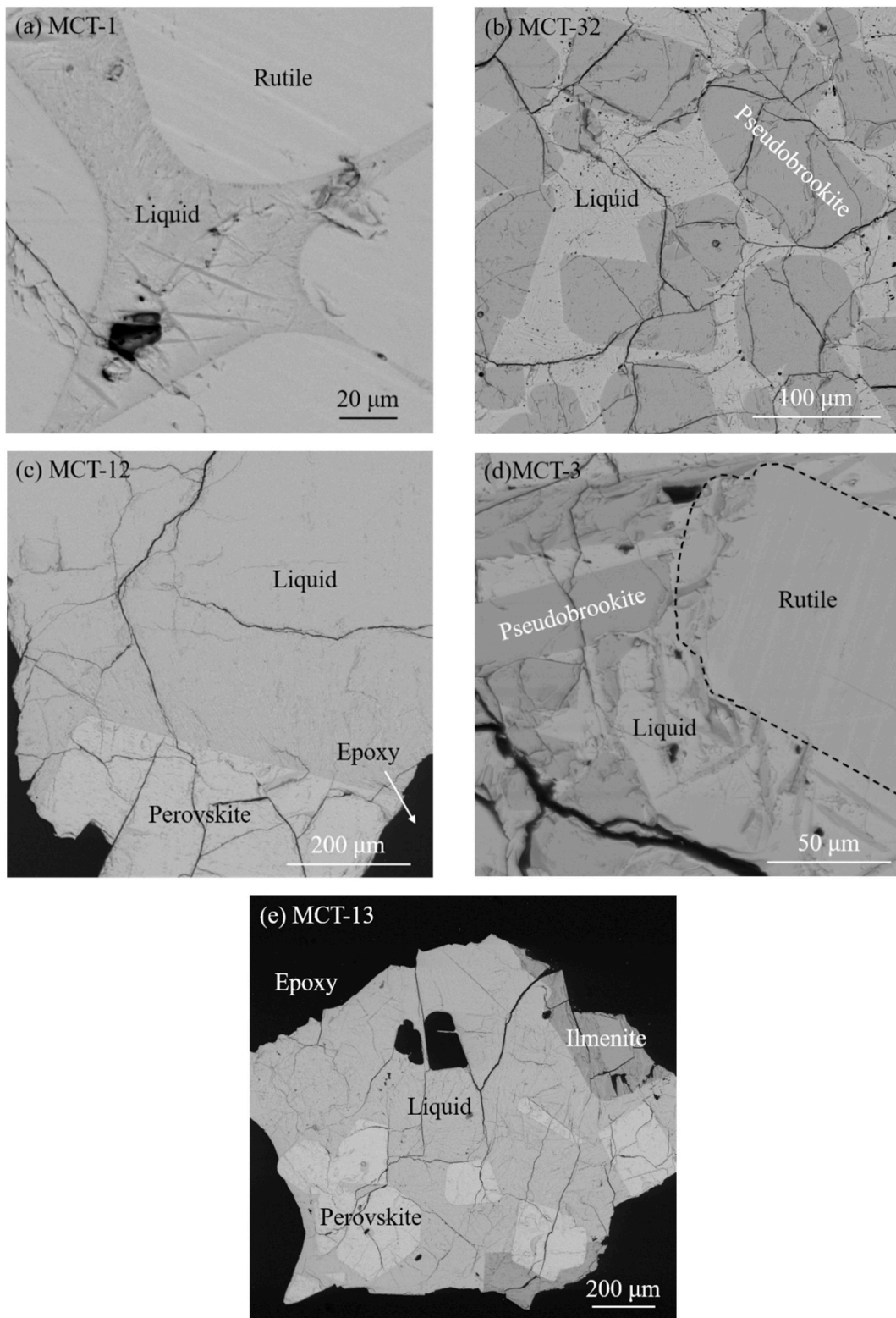


Fig. 2. Backscattered electron (BSE) images of typical samples obtained at 1500 °C; (a) liquid-rutile; (b) liquid-pseudobrookite; (c) liquid-perovskite; (d) liquid-pseudobrookite-rutile; (e) liquid-ilmenite-perovskite.

Table 1
Equilibrium phase compositions for the MgO–CaO–TiO₂ system in air at 1500 °C measured by EPMA.

Sample	Equilibrium Phases	Equilibrium Compositions/wt%		
		MgO	TiO ₂	CaO
Liquid + Rutile				
MTC-1	Liquid	3.45 ± 0.07	82.68 ± 0.39	13.87 ± 0.38
	Rutile	0.03 ± 0.01	99.95 ± 0.01	0.02 ± 0.01
MTC-2	Liquid	5.95 ± 0.03	83.10 ± 0.03	10.96 ± 0.02
	Rutile	0.04 ± 0.02	99.92 ± 0.02	0.03 ± 0.01
Liquid + Pseudobrookite				
MTC-6	Liquid	8.06 ± 0.15	78.21 ± 0.16	13.72 ± 0.21
	Pseudobrookite	19.88 ± 0.09	79.92 ± 0.11	0.20 ± 0.03
MTC-32	Liquid	6.82 ± 0.24	79.48 ± 0.19	13.70 ± 0.23
	Pseudobrookite	19.68 ± 0.16	80.19 ± 0.18	0.13 ± 0.03
MCT-33	Liquid	6.64 ± 0.33	79.73 ± 0.23	13.63 ± 0.55
	Pseudobrookite	19.91 ± 0.11	79.98 ± 0.11	0.11 ± 0.02
Liquid + Perovskite				
MCT-10	Liquid	4.19 ± 0.10	79.16 ± 0.21	16.65 ± 0.20
	Perovskite	0.20 ± 0.12	59.30 ± 0.11	40.49 ± 0.10
MCT-12	Liquid	11.00 ± 0.06	73.35 ± 0.07	15.65 ± 0.04
	Perovskite	0.30 ± 0.02	59.11 ± 0.13	40.59 ± 0.13
Liquid + Rutile + Pseudobrookite				
MCT-3	Liquid	6.07 ± 0.10	83.07 ± 0.09	10.86 ± 0.04
	Rutile	0.05 ± 0.01	99.94 ± 0.01	0.02 ± 0.00
	Pseudobrookite	19.67 ± 0.09	80.21 ± 0.09	0.11 ± 0.02
MCT-5	Liquid	6.40 ± 0.08	81.68 ± 0.06	11.92 ± 0.04
	Rutile	0.04 ± 0.03	99.94 ± 0.03	0.01 ± 0.01
	Pseudobrookite	19.71 ± 0.08	80.18 ± 0.08	0.10 ± 0.01
MCT-31	Liquid	6.31 ± 0.13	80.40 ± 0.18	13.29 ± 0.25
	Rutile	0.05 ± 0.01	99.93 ± 0.01	0.02 ± 0.01
	Pseudobrookite	19.85 ± 0.14	80.05 ± 0.13	0.10 ± 0.02
Liquid + Perovskite + Ilmenite				
MCT-13	Liquid	14.35 ± 0.26	71.16 ± 0.22	14.49 ± 0.38
	Perovskite	0.33 ± 0.06	59.29 ± 0.05	40.38 ± 0.10
	Ilmenite	32.29 ± 0.12	67.30 ± 0.09	0.41 ± 0.05

wt% CaO, and 19.75 wt% MgO–80.15 wt% TiO₂–0.11 wt% CaO for liquid, rutile, and pseudobrookite, respectively.

3.2. Equilibrium phase relations at 1600 °C

Fig. 3 presents typical BSE (back scattered electron) images of samples equilibrated at 1600 °C. The compositions of the different phases with standard deviations ($\pm 1\sigma$) are listed in Table 2. Like the results obtained at 1500 °C, the primary phase domains of rutile, pseudobrookite, perovskite were also observed at 1600 °C. However, the liquid-titania spinel two-phase coexisting equilibrium as well as the liquid-pseudobrookite-ilmenite and the liquid-ilmenite-titania spinel three-phase coexisting equilibrium, not observed at 1500 °C, were found at 1600 °C.

4. Discussion

Based on the present experimentally determined equilibrium liquid compositions, the 1500 °C and 1600 °C isotherms were constructed, as shown in Figs. 4 and 5, respectively. The present results were compared with the data from the literature [49], and with simulations by FactSage using the *FactPS* and *FToxid* databases [57,58] and by MTDATA using its *MTOX* database [59,60].

4.1. Construction of the 1500 °C isotherm

As shown in Fig. 4(a), the primary phase fields of rutile and perovskite were experimentally determined at 1500 °C in air. However, the domains for liquid-pseudobrookite and liquid-ilmenite primary phase fields were not completely constructed due to the limited number of the experimental sample compositions.

Fig. 4(b) displays the comparison of the present results with the data from the literature [49]. It can be seen that the dynamic observations by Rouf et al. [49] suggest a much wider liquid domain than the present results. The isotherms for the primary phase fields of perovskite determined in this study shifted to the region with a lower CaO content but with higher TiO₂ concentrations when compared with the literature data. As for the present isothermal results for the pseudobrookite primary phase field, they exhibited lower MgO concentrations than the findings by Rouf et al. [49].

Fig. 4(c) shows a comparison of the present results with the calculated isothermal section by FactSage. The liquid domain simulated by FactSage is larger than that of the present experimental results. The experimentally measured isotherm for the rutile primary phase field agrees well with the simulations by FactSage within the MgO range of 0–5 wt%. However, the liquid point for the liquid-rutile-pseudobrookite three-phase coexisting equilibrium determined in this study displays a composition with lower TiO₂ but higher CaO concentration when compared with the predictions by FactSage. The present isotherm for the

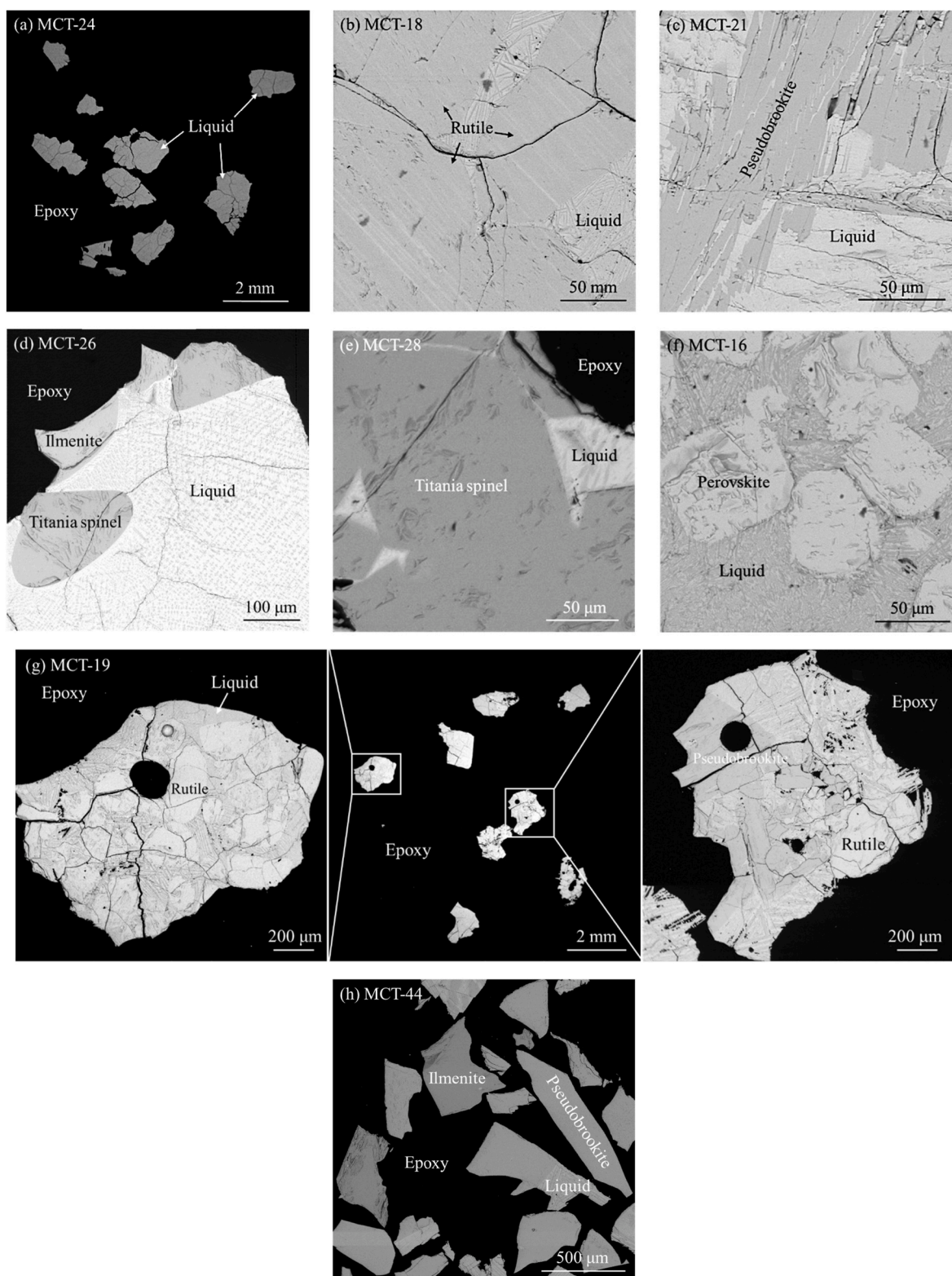


Fig. 3. Typical microstructures of liquid-solid and liquid-solid-solid coexisting equilibria obtained at 1600 °C; (a) single liquid; (b) liquid-rutile; (c) liquid-pseudobrookite; (d) liquid-ilmenite-titania spinel; (e) liquid-titania spinel; (f) liquid-perovskite; (g) liquid-pseudobrookite-rutile; (h) liquid-ilmenite-pseudobrookite.

Table 2
Equilibrium phase compositions for the MgO–CaO–TiO₂ system in air at 1600 °C obtained using EPMA.

Sample	Equilibrium Phases	Equilibrium Composition/wt%		
		MgO	TiO ₂	CaO
Single Liquid				
MTC-24	Liquid	10.60 ± 0.21	74.94 ± 0.21	14.47 ± 0.24
Liquid + Rutile				
MTC-17	Liquid	4.20 ± 0.10	84.64 ± 0.32	11.16 ± 0.27
	Rutile	0.04 ± 0.01	99.82 ± 0.09	0.13 ± 0.09
MTC-18	Liquid	7.88 ± 0.44	84.27 ± 0.46	7.84 ± 0.37
	Rutile	0.07 ± 0.02	99.89 ± 0.02	0.03 ± 0.03
MTC-43	Liquid	6.49 ± 0.13	84.21 ± 0.41	9.30 ± 0.32
	Rutile	0.05 ± 0.02	99.95 ± 0.02	0.00 ± 0.00
Liquid + Pseudobrookite				
MTC-21	Liquid	10.85 ± 0.16	82.50 ± 0.28	6.65 ± 0.42
	Pseudobrookite	19.60 ± 0.10	80.35 ± 0.10	0.04 ± 0.00
MTC-22	Liquid	12.36 ± 0.95	78.74 ± 0.31	8.90 ± 1.22
	Pseudobrookite	19.93 ± 0.07	80.01 ± 0.07	0.06 ± 0.00
Liquid + Titania spinel				
MCT-28	Liquid	22.26 ± 0.53	68.22 ± 0.33	9.21 ± 0.49
	Titania spinel	48.35 ± 0.16	51.45 ± 0.15	0.20 ± 0.01
Liquid + Perovskite				
MCT-15	Liquid	7.24 ± 0.04	73.41 ± 0.10	19.35 ± 0.10
	Perovskite	0.23 ± 0.02	59.03 ± 0.06	40.75 ± 0.06
MCT-16	Liquid	10.30 ± 0.11	71.23 ± 0.20	18.47 ± 0.15
	Perovskite	0.28 ± 0.02	59.22 ± 0.06	40.49 ± 0.07
MCT-40	Liquid	12.73 ± 0.20	70.95 ± 0.21	16.32 ± 0.39
	Perovskite	0.34 ± 0.03	59.28 ± 0.06	40.41 ± 0.09
MCT-41	Liquid	14.92 ± 0.22	67.85 ± 0.06	17.23 ± 0.25
	Perovskite	0.43 ± 0.03	59.06 ± 0.07	40.51 ± 0.07
Liquid + Rutile + Pseudobrookite				
MCT-19	Liquid	10.87 ± 0.95	84.22 ± 0.95	4.91 ± 0.53
	Rutile	0.08 ± 0.02	99.91 ± 0.02	0.01 ± 0.00
	Pseudobrookite	19.30 ± 0.08	80.65 ± 0.07	0.05 ± 0.01
Liquid + Ilmenite + Pseudobrookite				
MCT-44	Liquid	17.07 ± 0.20	72.13 ± 0.39	10.80 ± 0.58
	Pseudobrookite	19.76 ± 0.06	80.18 ± 0.05	0.06 ± 0.00
	Ilmenite	32.19 ± 0.06	67.55 ± 0.05	0.26 ± 0.01
Liquid + Ilmenite + Titania spinel				
MCT-26	Liquid	23.82 ± 0.20	68.75 ± 0.16	7.43 ± 0.15
	Ilmenite	32.61 ± 0.13	67.23 ± 0.14	0.16 ± 0.16
	Titania spinel	47.59 ± 0.29	52.24 ± 0.29	0.17 ± 0.04

pseudobrookite primary phase field shows a higher CaO concentration than the predictions by FactSage.

A comparison of the present results with the predictions by MTDATA shown in Fig. 4(d) indicates that the present experimentally determined liquid domain is smaller than the predictions by MTDATA. The present experimentally determined isotherms for the primary phase fields of rutile and pseudobrookite fitted well with the calculated results. The present results for the perovskite primary phase field shifted to the region with higher TiO₂ concentration. The presence of the liquid-perovskite-ilmenite three-phase equilibrium determined at 1500 °C in this study disproves the formation of the tie-lines for (liquid-titania spinel) and (liquid-monoxide) and the corresponding equilibria predicted by FactSage and MTDATA.

4.2. Construction of the 1600 °C isotherm

Fig. 5(a) shows the present experimentally determined 1600 °C isothermal section of the MgO–CaO–TiO₂ phase diagram in air. The primary phase fields of rutile and perovskite were also determined at 1600 °C, expanding toward the region with higher TiO₂ and CaO concentrations, respectively, when compared with the liquidus line obtained at 1500 °C. The liquid point for the liquid-rutile-pseudobrookite equilibrium shifted to the region with higher TiO₂ and MgO concentrations with the increase in temperature from 1500 °C to 1600 °C. The phase domain of ilmenite, which was not observed at 1500 °C, was

constructed successfully at 1600 °C. Due to the limited number of experimental points, the titania spinel phase field was not fully and reliably determined.

A comparison of the present results with the data from the literature, shown in Fig. 5(b), indicates that the present 1600 °C isotherm in the rutile primary phase field displayed a lower TiO₂ concentration than the previous observations [49]. However, the results for the perovskite primary phase field measured in the present study exhibited a relatively lower CaO but higher TiO₂ concentrations compared with the observations by Rouf et al. [49]. The present results for the pseudobrookite primary phase field had a slightly higher CaO concentration than those found by Rouf et al. [49]. The ilmenite phase field determined in this study is much narrower than the reported values in the literature, shifting toward the area with lower MgO but higher TiO₂ concentrations.

Fig. 5(c) shows that the liquid phase domain obtained in this study is narrower and smaller than that simulated by FactSage, shrinking toward the higher TiO₂ concentration corner. The present experimentally determined isotherm for the rutile primary phase exhibited lower TiO₂ concentrations than the predictions by FactSage. The present isotherm for the primary phase field of pseudobrookite had a higher CaO content than the FactSage predictions. The results in the perovskite primary phase field obtained in this study exhibited higher TiO₂ concentrations. The titania spinel phase domain simulated by FactSage and MTDATA is wider than the present experimental results, also displaying a much

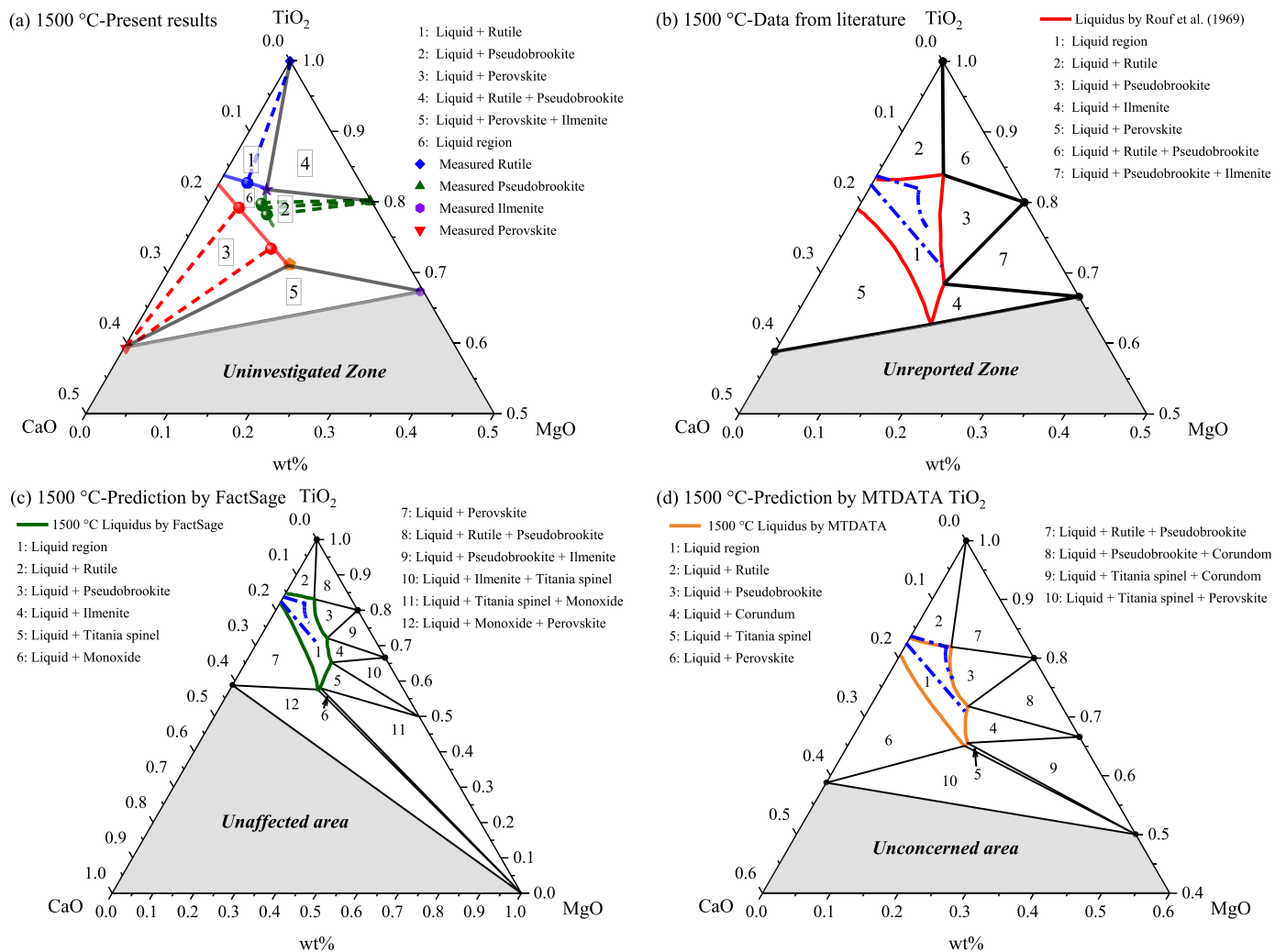


Fig. 4. Isothermal section of the CaO–MgO–TiO₂ system in air at 1500 °C: (a) the present results; (b) comparisons with the data from literature [49]; (c) predictions by FactSage; and (d) predictions by MTDATA. Corundum of MTDATA represents the same solution phase as ilmenite in the present study and in the FactSage predictions. The dash-dotted line in Fig. 4(b)–(d) represents the present experimental results obtained at 1500 °C.

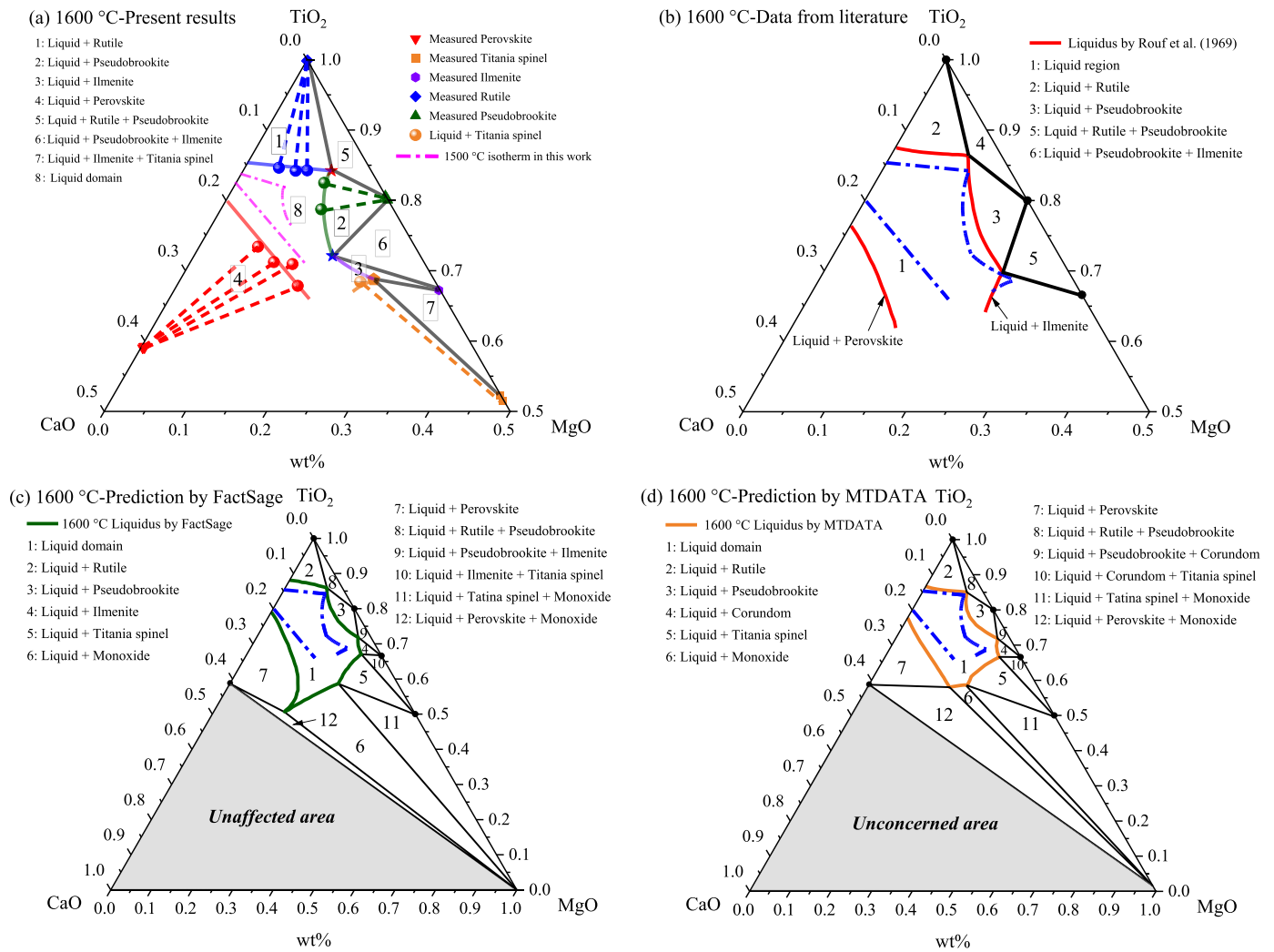


Fig. 5. Isothermal phase diagram of CaO–MgO–TiO₂ system in air at 1600 °C: (a) present results; (b) comparisons with the data from literature [49]; (c) predictions by FactSage; and (d) predictions by MTDATA. The dashed line in Fig. 5(b)–(d) represents the present experimental results obtained at 1600 °C.

higher MgO concentration.

Fig. 5(d) indicates that the liquid domain simulated by MTDATA deviated significantly from the present observations. The present experimentally determined isotherms in the rutile primary phase field agreed well with the predictions made by MTDATA. The simulated phase domains of pseudobrookite, corundum (i.e., ilmenite in the present study and by FactSage), and titania spinel are wider than that in the present observations and shifted to a higher TiO₂ but lower MgO concentration area. The predicted isotherm for the perovskite primary phase field shifted toward the area with higher CaO but lower TiO₂ concentration when compared with the present results. However, the predictions by FactSage and MTDATA fit well with the primary phase fields of rutile, pseudobrookite, and ilmenite.

5. Conclusions

The equilibrium phase relations of the MgO–CaO–TiO₂ system were experimentally investigated in air in the temperature range between 1500 °C and 1600 °C. The experimental methodology involved high-temperature isothermal equilibration of the samples followed by rapid quenching of the condensed equilibrium phases, and direct phase characterization by SEM-EDS and EPMA from polished sections. Observations were made of the liquid-solid primary phase equilibria of rutile, pseudobrookite, ilmenite, titania spinel, and perovskite as well as the three-phase equilibria of liquid-pseudobrookite-rutile, liquid-

pseudobrookite-ilmenite, liquid-ilmenite-titania spinel, and liquid-perovskite-ilmenite.

The 1500 °C and 1600 °C isothermal phase diagrams were constructed based on the experimentally determined liquid compositions, providing information for the selective crystallization of TiO₂-enriched rutile, pseudobrookite, ilmenite, titania spinel, and perovskite phases from titania-bearing blast furnace slags by adjusting the temperature or slag composition. The obtained results were compared with data from the literature and predictions by FactSage and MTDATA and the current data showed large discrepancies with them in the perovskite, pseudobrookite, and ilmenite primary phase fields. The present results will be used for the further optimization of phase equilibria in the higher-order CaO–SiO₂–Al₂O₃–MgO–TiO₂ systems.

Declaration of competing interest

The authors declare that they have no known competing financial interests or personal relationships that could have appeared to influence the work reported in this paper.

Acknowledgements

The use of the Academy of Finland's RawMatTERS Finland Infrastructure (RAMI), housed jointly at Aalto University, GTK, and VTT in Espoo, is greatly acknowledged. Min Chen is grateful for the financial

support from the China Scholarship Council (#201806370217). This work is partly financed by Aalto University, School of Chemical Engineering as well as the Natural Science Foundation of Liaoning Province (2021-MS-083). The authors would like to thank Ms. Fabiola Lasar and Mr. Kezhou Song for the assistance in experiments. Dr. Lassi Klemettinen is greatly acknowledged for his valuable discussion.

References

- [1] C. Veiga, J.P. Davim, A.J.R. Loureiro, Properties and applications of titanium alloys: a brief review, *Rev. Adv. Mater. Sci.* 32 (2) (2012) 133–148.
- [2] S.H. Shin, S.J. Kim, Production of high-purity TiO₂ powder from FeTiO₃ via high-temperature sulfurization, *JOM* 73 (5) (2021) 1531–1537, <https://doi.org/10.1007/s11837-021-04618-w>.
- [3] W. Kroll, The production of ductile titanium, *Trans. Electrochem. Soc.* 78 (1) (1940) 35, <https://doi.org/10.1149/1.3071290>.
- [4] D.J. Fray, Novel methods for the production of titanium, *Int. Mater. Rev.* 53 (6) (2008) 317–325, <https://doi.org/10.1179/174328008X324594>.
- [5] X. Wan, P. Taskinen, J. Shi, A. Jokilaakso, A potential industrial waste-waste co-treatment process of utilizing waste SO₂ gas and residue heat to recover Co, Ni, and Cu from copper smelting slag, *J. Hazard Mater.* 414 (2021), 125541, <https://doi.org/10.1016/j.jhazmat.2021.125541>.
- [6] X. Wan, J. Shi, P. Taskinen, A. Jokilaakso, Extraction of copper from copper-bearing materials by sulfation roasting with SO₂-O₂ gas, *JOM* 72 (10) (2020) 3436–3446, <https://doi.org/10.1007/s11837-020-04300-7>.
- [7] J. Shi, C. Peng, M. Chen, Y. Li, H. Eric, L. Klemettinen, M. Lundström, P. Taskinen, A. Jokilaakso, Sulfation roasting mechanism for spent lithium-ion battery metal oxides under SO₂-O₂-Ar atmosphere, *JOM* 71 (12) (2019) 4473–4482, <https://doi.org/10.1007/s11837-019-03800-5>.
- [8] M. Chen, K. Avarmaa, L. Klemettinen, H. O'Brien, D. Sukhomlinov, J. Shi, P. Taskinen, A. Jokilaakso, Recovery of precious metals (Au, Ag, Pt, and Pd) from urban mining through copper smelting, *Metall. Mater. Trans. B* 51 (4) (2020) 1495–1508, <https://doi.org/10.1007/s11663-020-01861-5>.
- [9] M. Chen, K. Avarmaa, L. Klemettinen, H. O'Brien, J. Shi, P. Taskinen, D. Lindberg, A. Jokilaakso, Precious metal distributions between copper matte and slag at high P_{SO2} in WEEE reprocessing, *Metall. Mater. Trans. B* 52 (2) (2021) 871–882, <https://doi.org/10.1007/s11663-021-02059-z>.
- [10] L. Zhang, W. Zhang, J. Zhang, G. Li, Oxidation kinetics and oxygen capacity of Ti-bearing blast furnace slag under dynamic oxidation conditions, *Metals* 6 (2016) 105, <https://doi.org/10.3390/met6050105>.
- [11] S. Ren, Q. Zhao, L. Yao, Q. Liu, Precipitation behavior of perovskite and anosovite crystals from high Ti-bearing blast furnace slag with small amount of B₂O₃, *CrystEngComm* 18 (2016) 1393–1402, <https://doi.org/10.1039/C5CE02131F>.
- [12] J. Han, J. Zhang, J. Zhang, X. Chen, L. Zhang, G. Tu, Combined effect of SiO₂ and O₂ on the crystallization behavior of modified Ti-bearing blast furnace slag, *ACS Omega* 5 (2020) 8619–8628, <https://doi.org/10.1021/acsomega.0c00014>.
- [13] J. Shi, Y. Qiu, B. Yu, X. Xie, J. Dong, C. Hou, J. Li, C. Liu, Titanium extraction from titania-bearing blast furnace slag: a review, *JOM* 74 (2022) 654–667, <https://doi.org/10.1007/s11837-021-05040-y>.
- [14] L. Zhang, W. Zhang, J. Zhang, G. Li, Oxidation kinetics and oxygen capacity of Ti-bearing blast furnace slag under dynamic oxidation conditions, *Metals* 6 (2016) 105, <https://doi.org/10.3390/met6050105>.
- [15] J. Li, X. Wang, Z. Zhang, Crystallization behavior of rutile in the synthesized Ti-bearing blast furnace slag using single hot thermocouple technique, *ISIJ Int.* 51 (9) (2011) 1396–1402, <https://doi.org/10.2355/isijinternational.51.1396>.
- [16] W. Zhang, L. Zhang, Y. Li, X. Li, An environmental procedure to extract titanium components and metallic iron from Ti-bearing blast furnace slag, *Green Process. Synth.* 4 (4) (2015) 307–316, <https://doi.org/10.1515/gps-2015-0031>.
- [17] L. Sun, J. Shi, Z. Yu, M. Jiang, Phase equilibria and liquidus surface of CaO-SiO₂-5 wt% MgO-Al₂O₃-TiO₂ slag system, *Ceram. Int.* 45 (1) (2019) 481–487, <https://doi.org/10.1016/j.ceramint.2018.09.193>.
- [18] M. Chen, J. Shi, P. Taskinen, A. Jokilaakso, Phase equilibria of the CaO-SiO₂-TiO₂-Al₂O₃-MgO system in air at 1250–1400 °C, *Ceram. Int.* 46 (17) (2020) 27702–27710, <https://doi.org/10.1016/j.ceramint.2020.07.268>.
- [19] J. Shi, M. Chen, X. Wan, P. Taskinen, A. Jokilaakso, Phase equilibrium study of the CaO-SiO₂-MgO-Al₂O₃-TiO₂ system at 1300 °C and 1400 °C in air, *JOM* 72 (9) (2020) 3204–3212, <https://doi.org/10.1007/s11837-020-04136-1>.
- [20] J. Shi, M. Chen, I. Santoso, L. Sun, M. Jiang, P. Taskinen, A. Jokilaakso, 1250 °C liquidus for the CaO-MgO-SiO₂-Al₂O₃-TiO₂ system in air, *Ceram. Int.* 46 (2) (2020) 1545–1550, <https://doi.org/10.1016/j.ceramint.2019.09.122>.
- [21] Z. Wang, Q. Zhu, H. Sun, Phase equilibria in the TiO₂-rich part of the TiO₂-CaO-SiO₂-10 Wt Pct Al₂O₃-5 Wt Pct MgO system at 1773 K, *Metall. Mater. Trans. B* 50 (1) (2019) 357–366, <https://doi.org/10.1007/s11663-018-1441-2>.
- [22] J. Shi, L. Sun, J. Qiu, M. Jiang, Phase equilibrium investigation for CaO-SiO₂-5wt.% MgO-20wt.% Al₂O₃-TiO₂ system relevant to Ti-bearing slag system, *ISIJ Int.* 58 (3) (2018) 431–438, <https://doi.org/10.2355/isijinternational.ISIJINT-2017-555>.
- [23] J. Shi, L. Sun, J. Qiu, M. Jiang, Phase equilibria of CaO-SiO₂-5wt.% MgO-30 wt.% Al₂O₃-TiO₂ system at 1400 °C and 1450 °C relevant to high Al₂O₃ Ti-bearing blast furnace slag system, *J. All. Comp.* 722 (2017) 25–32, <https://doi.org/10.1016/j.jallcom.2017.06.058>.
- [24] J. Shi, L. Sun, B. Zhang, X. Liu, J. Qiu, Z. Wang, M. Jiang, Experimental determination of the phase diagram of the CaO-SiO₂-5 pct MgO-10 pct Al₂O₃-TiO₂ system, *Metall. Mater. Trans. B* 47 (1) (2016) 425–433, <https://doi.org/10.1007/s11663-015-0527-3>.
- [25] J. Shi, L. Sun, J. Qiu, Z. Wang, B. Zhang, M. Jiang, Experimental determination of the phase diagram for CaO-SiO₂-MgO-10% Al₂O₃-5% TiO₂ system, *ISIJ Int.* 56 (7) (2016) 1124–1131, <https://doi.org/10.2355/isijinternational.ISIJINT-2016-045>.
- [26] L. Sun, J. Shi, C. Liu, M. Jiang, Phase equilibria studies for CaO-SiO₂-5wt.% MgO-Al₂O₃-TiO₂ system in high Al₂O₃ content area with w(CaO)/w(SiO₂) ratio of 1.50, *J. All. Comp.* 810 (2019), 151949, <https://doi.org/10.1016/j.jallcom.2019.151949>.
- [27] L.F. Sun, J.J. Shi, B. Zhang, J.Y. Qiu, Z.Y. Wang, M.F. Jiang, Liquidus and phase equilibria in CaO-SiO₂-5% MgO-20% Al₂O₃-TiO₂ system, *J. Central South Univ.* 24 (1) (2017) 48–55, <https://doi.org/10.1007/s11771-017-3407-y>.
- [28] M. Chen, J. Shi, P. Taskinen, A. Jokilaakso, Experimental determination of the 1300 °C and 1400 °C isotherms for CaO-SiO₂-TiO₂-10 wt% Al₂O₃ system in air, *Ceram. Int.* 46 (7) (2020) 9183–9191, <https://doi.org/10.1016/j.ceramint.2019.12.170>.
- [29] Z. Wang, X. Liu, L. Zhang, Q. Zhu, The influence of composition on crystallization and liberation behavior of Ti-rich phase in Ti-bearing slags, *Indian Inst. Met.* 69 (1) (2016) 97–105, <https://doi.org/10.1007/s12666-015-0720-8>.
- [30] X.D. Wang, Y.W. Mao, X.Y. Liu, Y.K. Zhu, Study on crystallization behavior of blast furnace slag containing TiO₂, *J. Iron and Steel Res. Int.* 3 (1990) 1–6.
- [31] Y. Sun, J. Li, X. Wang, Z. Zhang, The effect of P₂O₅ on the crystallization behaviors of Ti-bearing blast furnace slags using single hot thermocouple technique, *Metall. Mater. Trans. B* 45 (4) (2014) 1446–1455, <https://doi.org/10.1007/s11663-014-0077-0>.
- [32] L. Sun, J. Shi, Z. Yu, M. Jiang, Phase equilibria and liquidus surface of CaO-SiO₂-5 wt% MgO-Al₂O₃-TiO₂ slag system, *Ceram. Int.* 45 (1) (2019) 481–487, <https://doi.org/10.1016/j.ceramint.2018.09.193>.
- [33] G.A. Rankin, H.E. Merwin, The ternary system CaO-Al₂O₃-MgO, *J. Am. Chem. Soc.* 38 (3) (1916) 568–588.
- [34] R.C. Doman, J.B. Barr, R.N. McNally, A.M. Alper, Phase equilibria in the system CaO-MgO, *J. Am. Ceram. Soc.* 46 (7) (1963) 313–316, <https://doi.org/10.1111/j.1151-2916.1963.tb11737.x>.
- [35] M. Hillert, W. Xizhen, Thermodynamic calculation of the CaO-MgO system, *Calphad* 13 (3) (1989) 267–271, [https://doi.org/10.1016/0364-5916\(89\)90006-0](https://doi.org/10.1016/0364-5916(89)90006-0).
- [36] J. Zhanpeng, D. Yong, A reassessment of the CaO-MgO system, *Calphad* 16 (1) (1992) 33–36, [https://doi.org/10.1016/0364-5916\(92\)90035-V](https://doi.org/10.1016/0364-5916(92)90035-V).
- [37] Y. Yin, B.J.B. Argent, The phase diagrams and thermodynamics of the ZrO₂-CaO-MgO and MgO-CaO systems, *J. Phase Equil.* 14 (5) (1993) 588–600, <https://doi.org/10.1007/BF02669140>.
- [38] P. Wu, G. Eriksson, A.D. Pelton, Critical evaluation and optimization of the thermodynamic properties and phase diagrams of the CaO-FeO, CaO-MgO, CaO-MnO, FeO-MgO, FeO-MnO, and MgO-MnO systems, *J. Am. Ceram. Soc.* 76 (8) (1993) 2065–2075, <https://doi.org/10.1111/j.1151-2916.1993.tb08334.x>.
- [39] W. Huang, M. Hillert, X. Wang, Thermodynamic assessment of the CaO-MgO-SiO₂ system, *Metall. Mater. Trans.* 26 (9) (1995) 2293–2310, <https://doi.org/10.1007/BF02671244>.
- [40] S. Serena, M.A. Sainz, S. De Aza, A. Caballero, Thermodynamic assessment of the system ZrO₂-CaO-MgO using new experimental results: calculation of the isoplethal section MgO-CaO-ZrO₂, *J. Eur. Ceram. Soc.* 25 (5) (2005) 681–693, <https://doi.org/10.1016/j.jeurceramsoc.2004.02.011>.
- [41] S.M. Liang, R. Schmid-Fetzer, Complete thermodynamic description of the Mg-Ca-O phase diagram including the Ca-O, Mg-O and CaO-MgO subsystems, *J. Eur. Ceram. Soc.* 38 (14) (2018) 4768–4785, <https://doi.org/10.1016/j.jeurceramsoc.2018.06.015>.
- [42] A. Jongejan, A.L. Wilkins, A re-examination of the system CaO-TiO₂ at liquidus temperatures, *J. Less Common. Met.* 20 (4) (1970) 273–279, [https://doi.org/10.1016/0022-5088\(70\)90001-9](https://doi.org/10.1016/0022-5088(70)90001-9).
- [43] W. Gong, L. Wu, A. Navrotsky, Combined experimental and computational investigation of thermodynamics and phase equilibria in the CaO-TiO₂ system, *J. Am. Ceram. Soc.* 101 (3) (2018) 1361–1370, <https://doi.org/10.1111/jace.15286>.
- [44] I. Shindo, Determination of the phase diagram by the slow cooling float zone method: the system MgO-TiO₂, *J. Cryst. Growth* 50 (4) (1980) 839–851, [https://doi.org/10.1016/0022-0248\(80\)90146-3](https://doi.org/10.1016/0022-0248(80)90146-3).
- [45] F. Massazza, E. Sircchia, The system MgO-SiO₂-TiO₂. I. Revision of the binary systems, *Chim. Ind.* 40 (1958) 376–380 (In Italian).
- [46] E. Woermann, B. Brezney, A. Muan, Phase equilibria in the system MgO-iron oxide-TiO₂ in air, *Am. J. Sci.* 267 (1969) 463–479.
- [47] G. Eriksson, A.D. Pelton, Critical evaluation and optimization of the thermodynamic properties and phase diagrams of the MnO-TiO₂, MgO-TiO₂, FeO-TiO₂, Ti₂O₃-TiO₂, Na₂O-TiO₂, and K₂O-TiO₂ systems, *Metall. Trans. A* B 24 (5) (1993) 795–805, <https://doi.org/10.1007/BF02663140>.
- [48] L.W. Coughanour, R.S. Roth, S. Marzullo, F.E. Sennett, Solid state reactions and dielectric properties in the system magnesite-lime-tin oxide-titania, *J. Res. Natl. Bur. Stand.* 54 (3) (1955) 149–162.
- [49] M.A. Rouf, A.H. Cooper, H.B. Bell, A study of phase equilibria in the system CaO-MgO-TiO₂, *Trans. J. Br. Ceram. Soc.* (1969) 263–267.
- [50] R.L. Shultz, Effects of titanium oxide on equilibria among refractory phases in the system CaO-MgO-iron oxide, *J. Am. Ceram. Soc.* 56 (1) (1973) 33–36, <https://doi.org/10.1111/j.1151-2916.1973.tb12346.x>.
- [51] M. Chen, X. Wan, J. Shi, P. Taskinen, A. Jokilaakso, Experimental study on the phase relations of the SiO₂-MgO-TiO₂ system in air at 1500 °C, *JOM* 74 (2022) 676–688, <https://doi.org/10.1007/s11837-021-04870-0>.

- [52] J. Shi, Y. Qiu, X. Wan, B. Yu, M. Chen, F. Zhao, J. Li, C. Liu, P. Taskinen, Equilibrium phase relations of CaO-SiO₂-Ti₃O₅ system at 1400 °C and p(O₂) of 10⁻¹⁶ atm, *JOM* 74 (2022) 668–675, <https://doi.org/10.1007/s11837-021-05049-3>.
- [53] X. Wan, M. Chen, Y. Qiu, J. Shi, J. Li, C. Liu, P. Taskinen, A. Jokilaakso, Influence of manganese oxide on the liquid-perovskite equilibrium in the CaO-SiO₂-TiO₂ system at 1400 °C in air, *Ceram. Int.* 47 (8) (2021) 11176–11182, <https://doi.org/10.1016/j.ceramint.2020.12.241>.
- [54] X. Wan, J. Shi, Y. Qiu, M. Chen, J. Li, C. Liu, P. Taskinen, A. Jokilaakso, The effect of 15 wt% Al₂O₃ addition on the equilibrium phase relations of CaO-SiO₂-TiO₂ system at 1400 °C in air, *Ceram. Int.* 47 (17) (2021) 24802–24808, <https://doi.org/10.1016/j.ceramint.2021.05.205>.
- [55] J.L. Pouchou, F. Pichoir, Basic expression of “PAP” computation for quantitative EPMA, in: J.D. Brown, R.H. Packwood (Eds.), In: *11th International Congress on X-Ray Optics and Microanalysis (ICXOM)*, 1986, pp. 249–253.
- [56] F.A. Hummel, in: M. Dekker (Ed.), *Introduction to Phase Equilibria in Ceramic Systems*, Routledge, Boca Raton, 2018.
- [57] C.W. Bale, E. Bélisle, P. Chartrand, S.A. Deckerov, G. Eriksson, K. Hack, I.H. Jung, Y.B. Kang, J. Melançon, A.D. Pelton, C. Robelin, S. Petersen, FactSage thermochemical software and databases-recent developments, *Calphad* 33 (2) (2009) 295–311, <https://doi.org/10.1016/j.calphad.2008.09.009>.
- [58] I.H. Jung, M.A. Van Ende, Computational thermodynamic calculations: FactSage from CALPHAD thermodynamic database to virtual process simulation, *Metall. Mater. Trans. B* 51 (5) (2020) 1851–1874, <https://doi.org/10.1007/s11663-020-01908-7>.
- [59] R.H. Davies, A.T. Dinsdale, J.A. Gisby, J.A.J. Robinson, A.M. Martin, MTDATA-thermodynamic and phase equilibrium software from the national physical laboratory, *Calphad* 26 (2) (2002) 229–271, [https://doi.org/10.1016/S0364-5916\(02\)00036-6](https://doi.org/10.1016/S0364-5916(02)00036-6).
- [60] J. Gisby, P. Taskinen, J. Pihlasalo, Z. Li, M. Tyrer, J. Pearce, K. Avarmaa, P. Björklund, H. Davies, M. Korpi, S. Martin, L. Pesonen, J. Robinson, MTDATA and the prediction of phase equilibria in oxide systems: 30 years of industrial collaboration, *Metall. Mater. Trans. B* 48 (1) (2017) 91–98, <https://doi.org/10.1007/s11663-016-0811-x>.